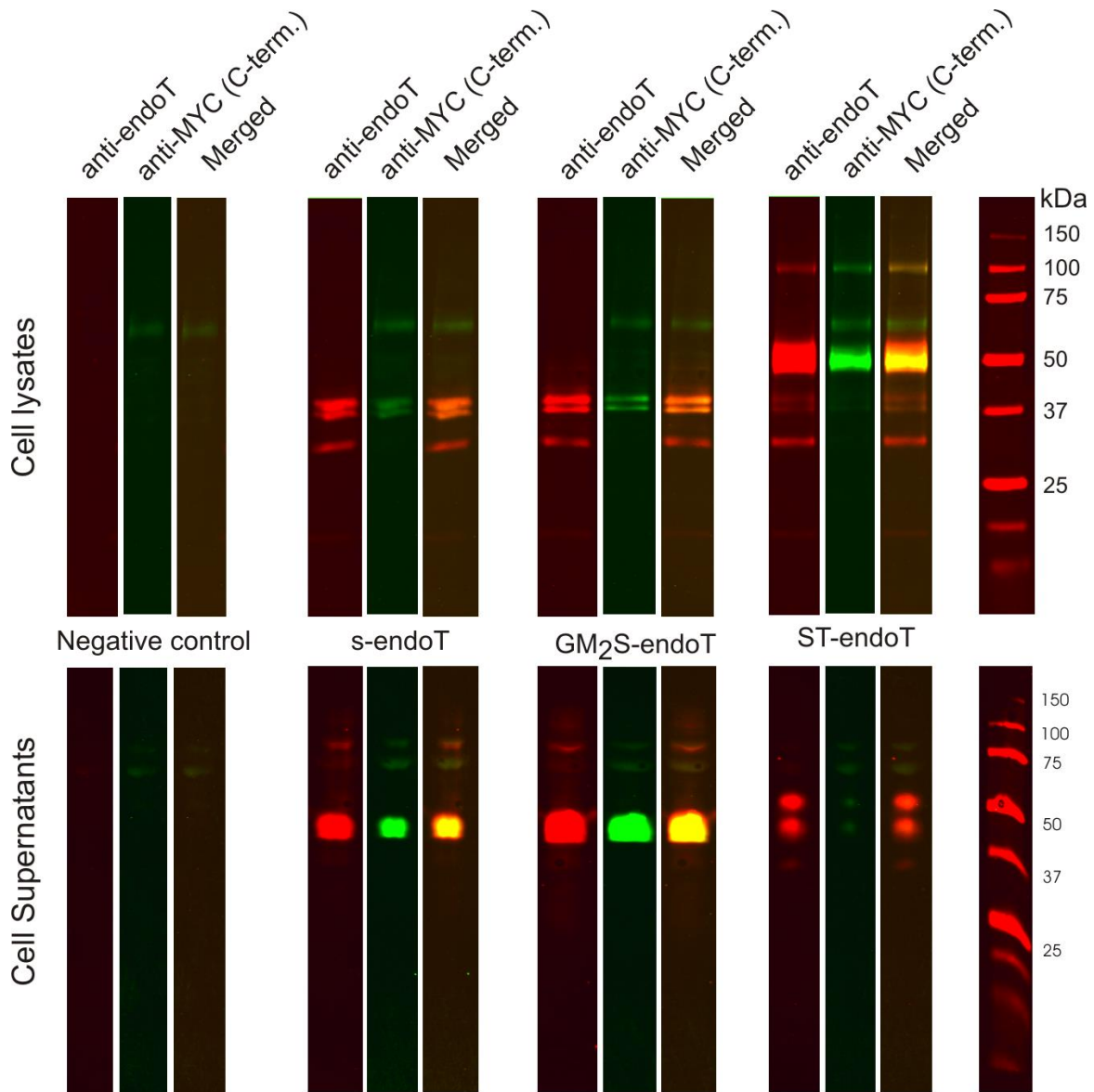


Supplementary Materials

| | |
|--|----|
| Supplementary Figure 1 | 2 |
| Supplementary Figure 2 | 3 |
| Supplementary Figure 3 | 4 |
| Supplementary Figure 4 | 5 |
| Supplementary Figure 5 | 6 |
| Supplementary Figure 6 | 7 |
| Supplementary Figure 7 | 8 |
| Supplementary Figure 8 | 9 |
| Supplementary Figure 9 | 10 |
| Supplementary Figure 10 | 11 |
| Supplementary Figure 11 | 12 |
| Supplementary Figure 12 | 14 |
| Supplementary Figure 13 | 15 |
| Supplementary Figure 14 | 16 |
| Supplementary Figure 15 | 17 |
| Supplementary table 1 | 19 |
| Supplementary table 2 | 20 |
| Supplementary table 3 | 21 |
| Supplementary table 4 | 22 |
| Supplementary table 5 | 23 |
| Supplementary table 6 | 24 |
| Supplementary table 7 | 26 |
| Supplementary table 8 | 27 |
| Supplementary Methods..... | 28 |
| Supplementary Note 1: Primer sequences | 33 |
| Supplementary Note 2: Methods gene expression analysis | 33 |
| Supplementary Note 3: Plasmid construction and protein purification | 34 |
| Supplementary Note 4: Methods in-gel tryptic digest..... | 35 |
| Supplementary Note 5: Calculations ratio of sialylated or galactosylated glycans | 36 |
| Supplementary Note 6: Biolayer interferometry assay. | 37 |
| References..... | 38 |

Supplementary Figure 1

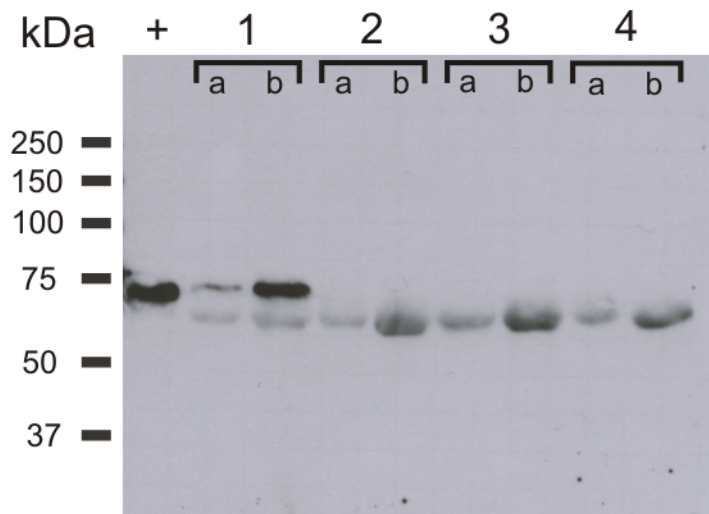
Evaluation of the two different *trans*-Golgi targeting domains (GM₂S-endoT and ST-endoT) compared to secreted endoT (s-endoT).



Supplementary Fig. 1. In this experiment we evaluated which of two *trans*-Golgi targeting sequences is most effective at retaining a fusion of these sequences with the endoT catalytic domain inside 293SGnT1^{-/-} cells. For comparison, we also analysed a secreted version of endoT (i.e. with a secretion signal but no Golgi targeting sequences). The western blots of SDS-PAGE separated cell lysate proteins and of proteins present in the cell cultivation medium were developed with a polyclonal anti-endoT antiserum or with a monoclonal anti-c-Myc epitope antibody. The c-Myc epitope is C-terminally fused to the different protein constructs and its presence or absence thus allows to conclude on C-terminal processing of the proteins. From these results it is clear that the GM₂S-derived sequence is ineffective at retaining endoT intracellularly, as this construct yields the same distribution of intra- and extracellular endoT forms as the secreted version of the protein. It appears that the GM₂ sequence is efficiently cleaved off. To the contrary, the ST-derived sequence effectively retains endoT intracellularly and the major band at 50 kDa matches the expected molecular mass of the ST-endoT fusion protein. Some minor secretion still occurs of two C-terminally proteolysed forms. The weak intracellular band that can be observed at 100 kDa probably represents ST-endoT dimers, since the ST6GalI domain is known to oligomerize¹.

Supplementary Figure 2

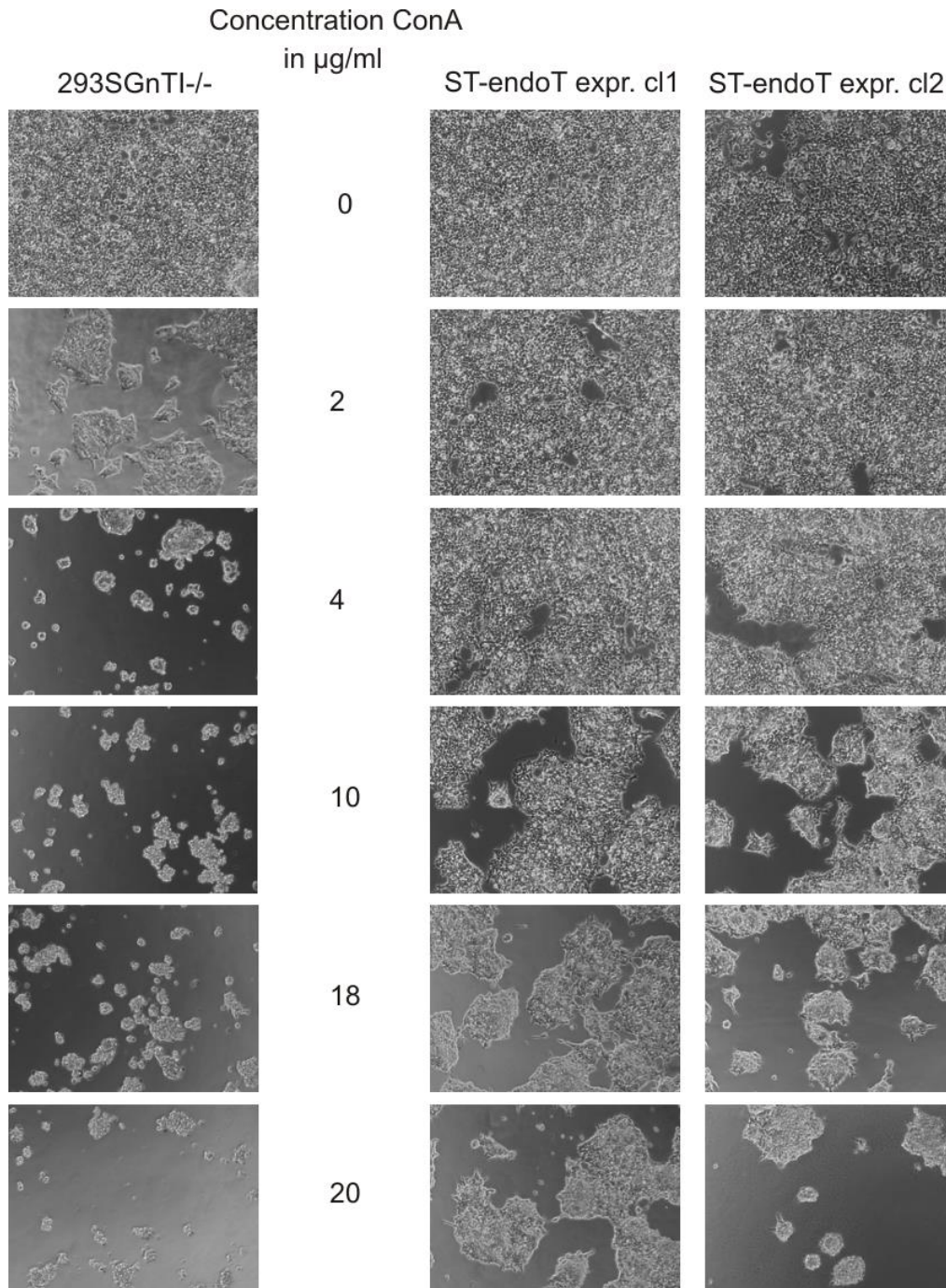
In vivo de-N-glycosylation by transient transfection of the endoT fusion constructs.



Supplementary Fig. 2. To evaluate the de-N-glycosylation by the endoT fusion proteins, the fusion constructs were transiently transfected to 293SGnTI^{-/-} cells that stably and inducibly expressed the Flt3 receptor extracellular domain (Flt3ECD). Samples were analysed by immunoblotting to detect the C-terminal His-tag. The numbers represent samples from cells transfected with 1 = empty plasmid, 2 = s-endoT plasmid, 3 = GM₂S-endoT plasmid, 4 = ST-endoT plasmid. Letters a and b in represent sample/supernatant 48 and 72 hours after transfection/induction. The + sign indicates Flt3ECD purified from non-engineered 293SGnTI^{-/-} cells as a positive control. It is evident from these blots that Flt3ECD shows a reduction in molecular weight upon transfection of any of the endoT constructs (2, 3, 4), but not with the empty plasmid (1), indicating de-N-glycosylation by the endoT fusion constructs. Clearly, deglycosylation by endoT can occur whether it is retained intracellularly (ST-endoT) or not (s-endoT and GM₂S-endoT). In further work we used the intracellular retained ST-endoT construct to enable further modification of the single GlcNAc generated by endoT by endogenous cellular glycosyltransferases (for retention behaviour of the constructs: see Supplementary Fig. 1).

Supplementary Figure 3

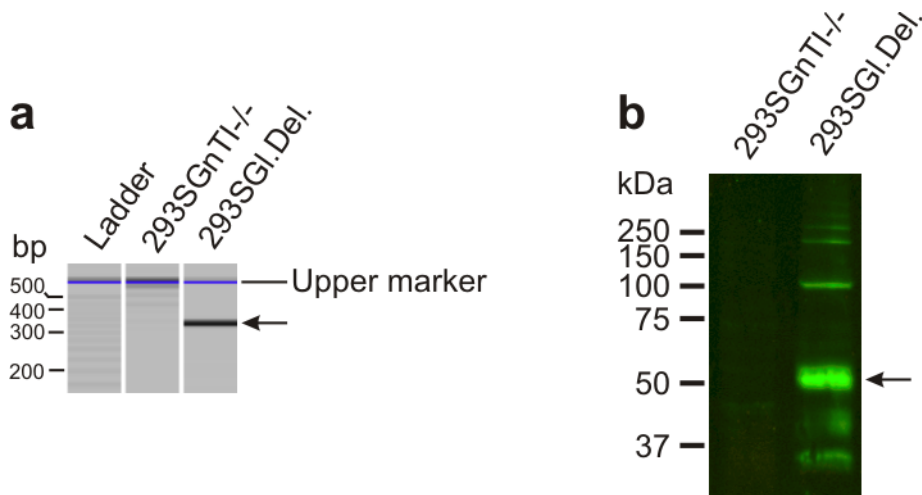
ConA sensitivity assay² for two ST-endoT overexpressing clones and the parental 293SGnTI^{-/-} line.



Supplementary Fig. 3. We performed a lectin sensitivity assay to determine the ConA sensitivity of 293SGnTI^{-/-} cells and two endoT overexpressing clones. Both clones were much more resistant to ConA than the parental line (at 2mg/ml or higher, all 293SGnTI^{-/-} were dead). However, the first clone was more resistant to ConA (>20 $\mu\text{g/ml}$) than the second clone (18 $\mu\text{g/ml}$), and was thus selected for further work. It was designated 293SGlycoDelete. The stability of the 293SGlycoDelete line's resistance to ConA was tested over 20 passages and was found to be stable (data not shown). Higher concentrations than about 20 $\mu\text{g/ml}$ could not be tested, because molecular aggregates started to form.

Supplementary Figure 4

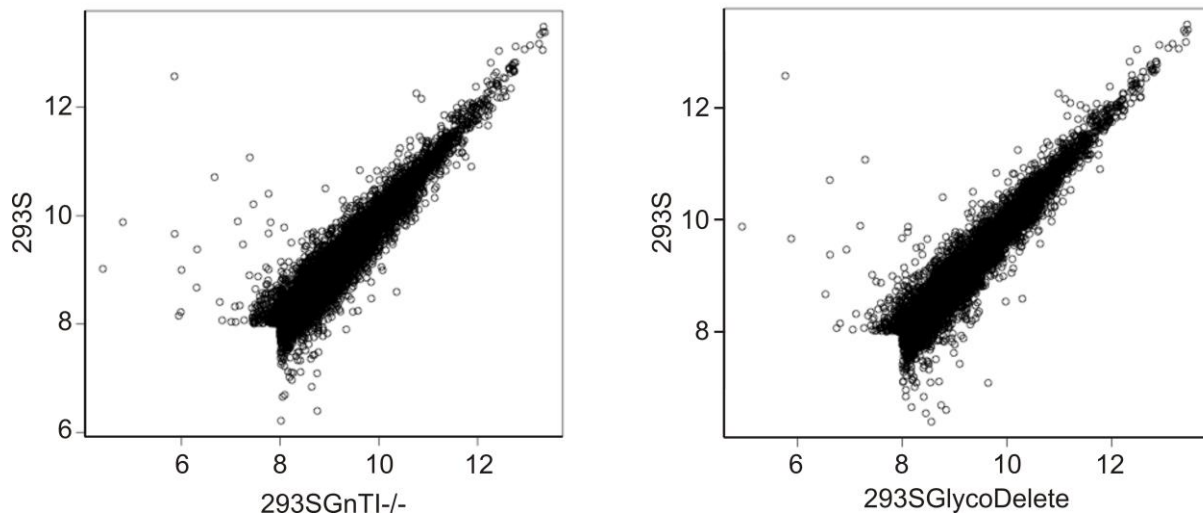
293SGlycoDelete cell line: validation of endoT genome integration by PCR and ST-endoT expression by western blot.



Supplementary Fig.4. Panel a: PCR validation of the presence of the ST-endoT coding sequence in 293SGlycoDelete cells genomic DNA (gDNA). Both the forward and reverse primer were designed to hybridize to the coding sequence of endoT (see Supplementary Note 2: P11 and P12). Analysis of the PCR products by capillary electrophoresis illustrates the presence of a specific PCR product of the expected length (346 bp) with 293SGlycoDelete gDNA as the template (arrow). This amplicon is not generated with 293SGnTI^{-/-} gDNA as the template for the PCR reaction. **Panel b:** Samples from 293SGnTI^{-/-} and 293SGlycoDelete cells were analysed by immunoblotting to detect the presence of endoT catalytic domain (polyclonal rabbit anti-endoT). The main band in the 293SGlycoDelete cell lysate runs at the expected MW of monomeric ST-endoT (49.8 kDa). Bands at approximately 100 and 200 kDa in the 293SGlycoDelete cell lysate are probably oligomers while bands at lower MW likely represent degradation products. The oligomers are also observed in transient transfection experiments with the ST-endoT construct (Supplementary Fig. 1). No signals for these bands can be detected in the negative control 293SGnTI^{-/-} lysate.

Supplementary Figure 5

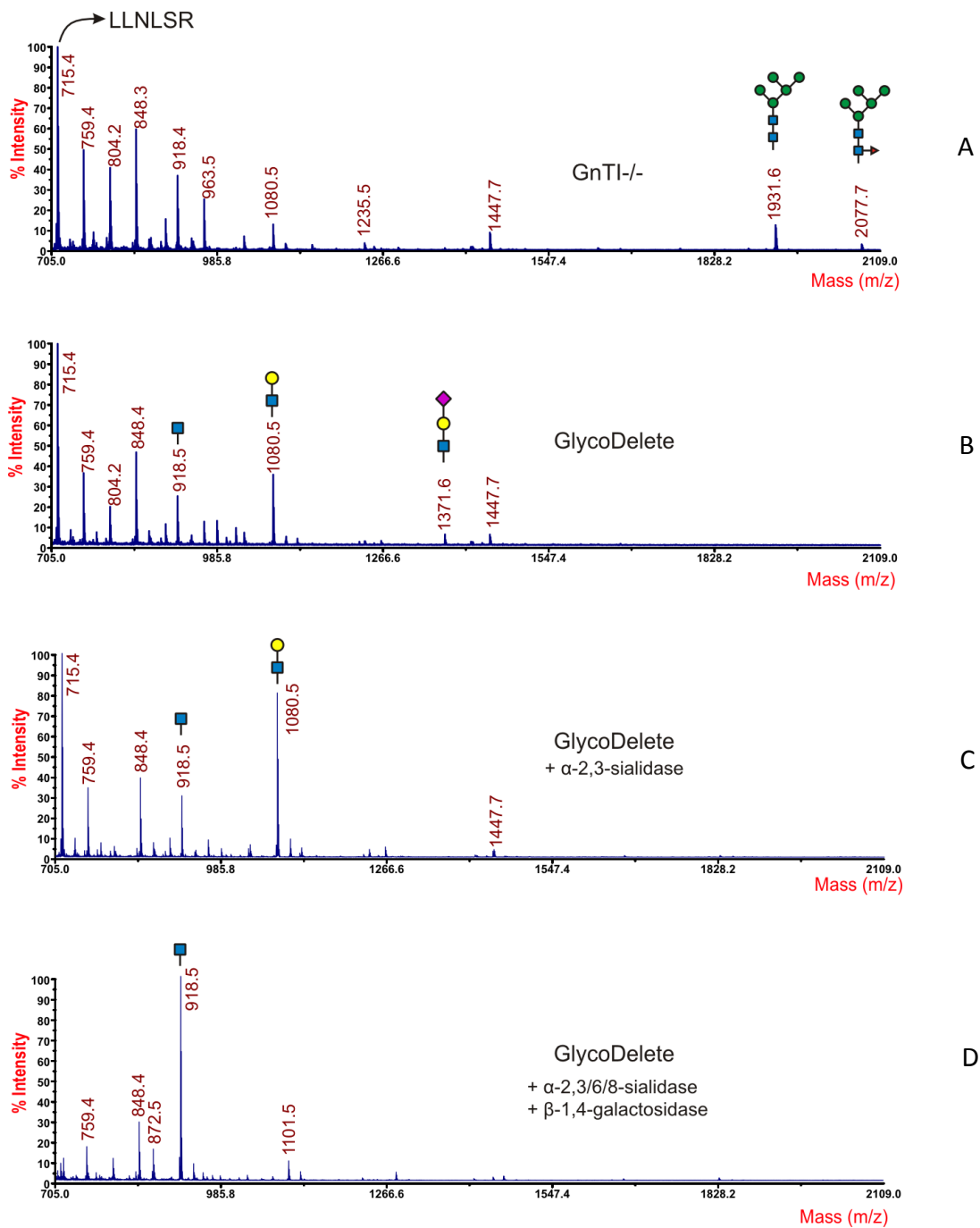
Comparative expression scatterplots of the S-lineage cell lines.



Supplementary Figure 5: Values represent the mean log₂ signal intensities of expressed genes as determined after background correction and removal of noise. Panel A: 293SGnTI^{-/-} versus 293S. The correlation coefficient is 0.947. From the 7526 expressed genes, 68 were found to be significantly differentially expressed ($p < 0.01$) with at least a two-fold change in expression in the 293SGnTI^{-/-} line compared with 293S. Panel B: 293SGlycoDelete vs 293S. The correlation coefficient is 0.938. From the 7473 expressed genes, 70 were found to be significantly differentially expressed ($p < 0.01$) with at least a two-fold change in expression in the 293SGlycoDelete line compared with 293S. Of these genes, 45 (-/+ 65%) are the same for both the derived cell lines versus the parental 293S cells. For detailed methods see Supplementary Note 2.

Supplementary Figure 6

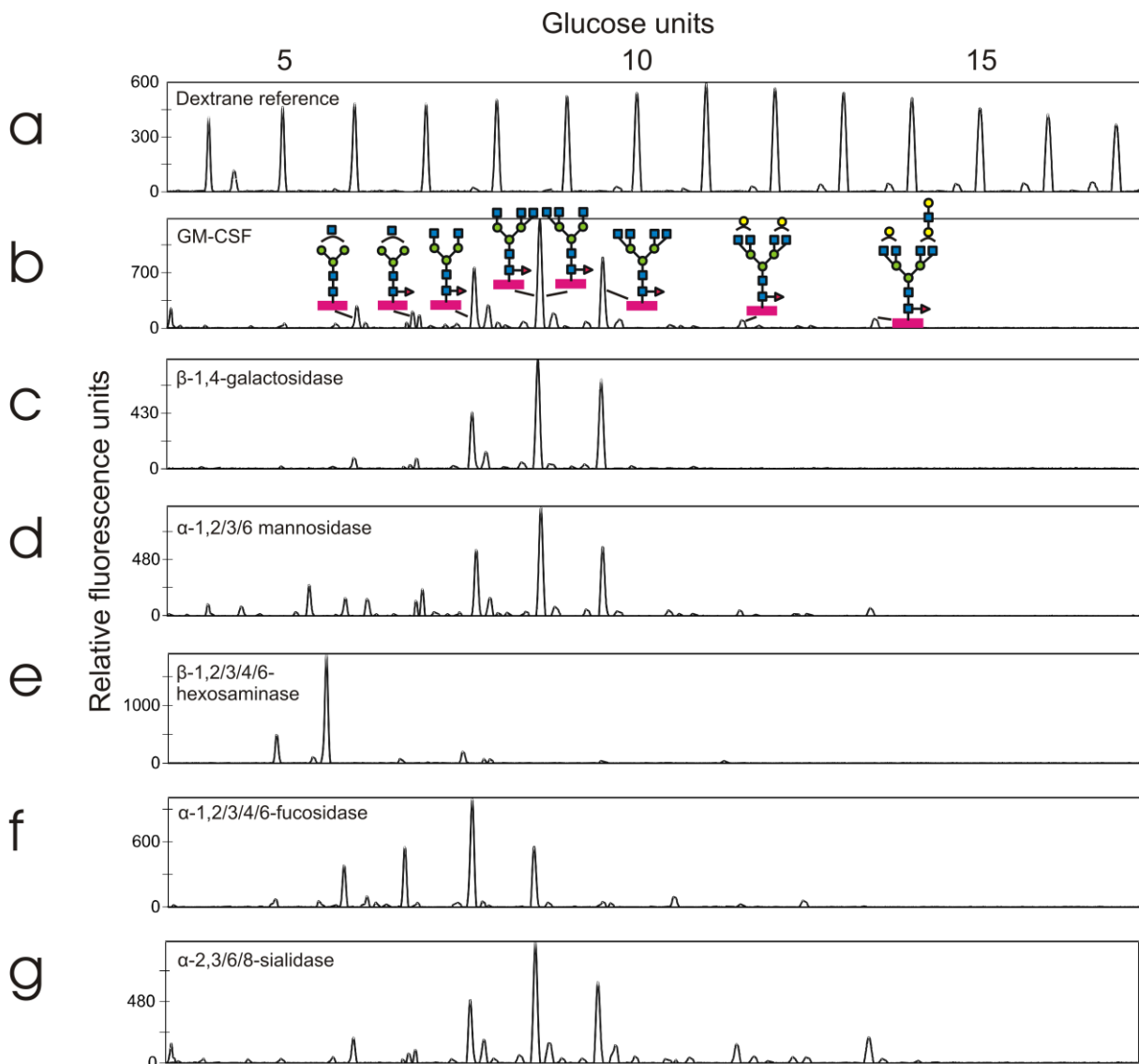
MALDI-TOF-MS of GM-CSF glycopeptides.



Supplementary Fig. 6. Glycopeptides encompassing Asn 27 in both lines, showing the presence of $\text{Man}_5\text{GlcNAc}_2\text{-Asn}$ ($m/z = 1931.6$) and fucosylated $\text{Man}_5\text{GlcNAc}_2\text{-Asn}$ ($m/z = 2077.7$) in GnTI^{-/-} GM-CSF (Panel A). These glycoforms are absent in GlycoDelete GM-CSF (Panel B). Peaks at $m/z = 918.5$, 1080.5 and 1371.6 are detected in GlycoDelete GM-CSF, representing HexNAc-Asn, Hex-HexNAc-Asn and Sia-Hex-HexNAc-Asn, respectively. Analysis of exoglycosidase-digested GlycoDelete GM-CSF N-glycans with α -2,3-sialidase (Panel C) or both a broad spectrum *A. ureafaciens* sialidase and *S. pneumoniae* β -1,4-galactosidase (Panel D) are shown. The spectra illustrate that the N-glycans on GlycoDelete GM-CSF are Neu5Ac- α -2,3-Gal- β -1,4-GlcNAc-Asn and Gal- β -1,4-GlcNAc-Asn.

Supplementary Figure 7

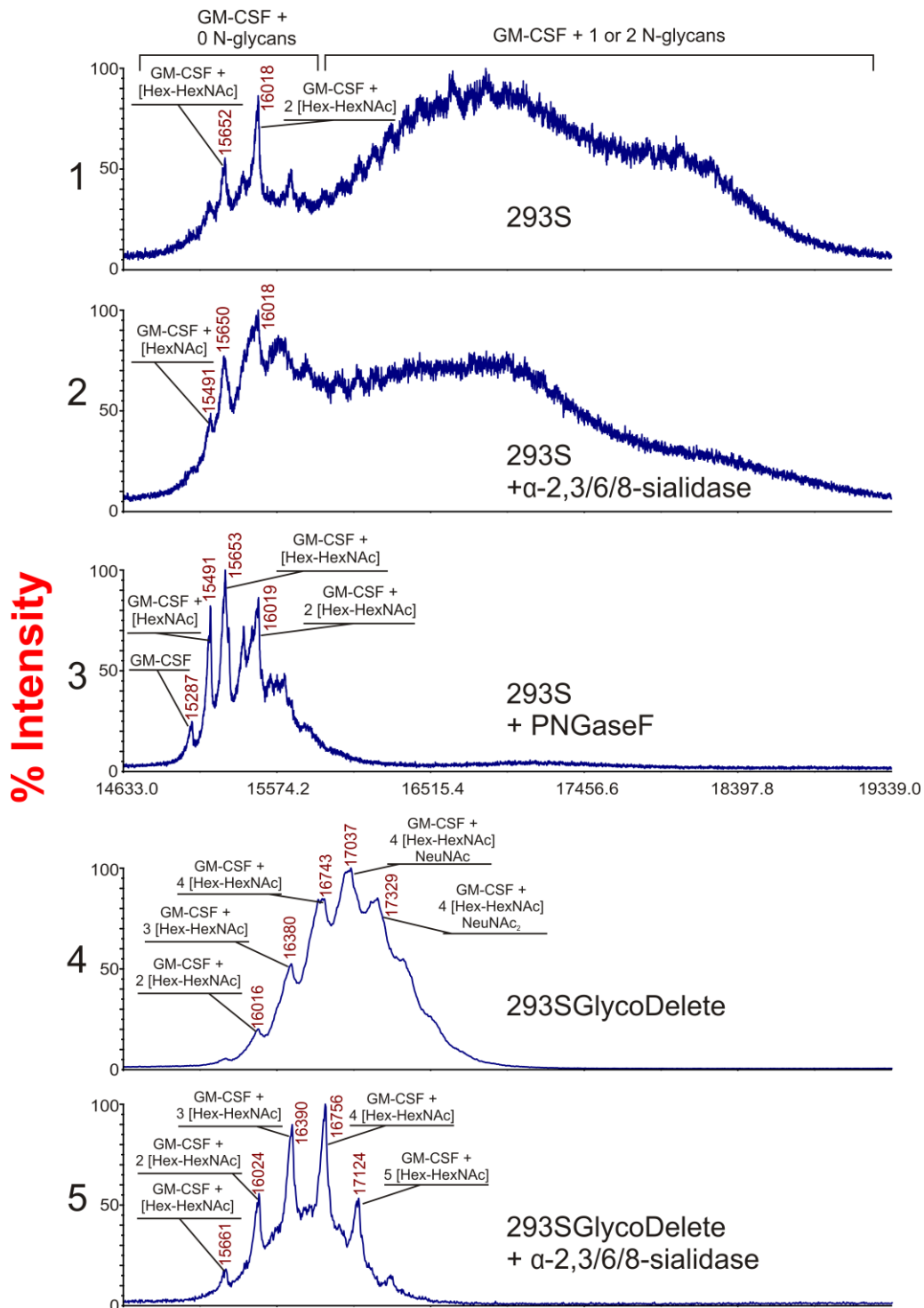
DSA-FACE analysis of GM-CSF produced in 293S cells.



Supplementary Fig. 7. Panel a: dextran ladder reference. **Panel b:** DSA-FACE profile of untreated GM-CSF produced in 293S cells with annotated structures. Glycosylation of GM-CSF produced in 293S cells results in a heterogeneous mix of mainly di-tri- and tetraantennary fucosylated complex type N-glycans without galactosylation. At lower electrophoretic mobility some galactosylated structures are observed. **Panel c:** Galactosylated structures disappear from the spectrum upon galactosidase digestion. **Panel d:** Two minor annotated peaks at the highest electrophoretic mobility collapse to a single peak with even higher electrophoretic mobility after mannosidase digestion. No further major changes occur after mannosidase digestion indicating little terminal mannose residues are exposed. **Panel e:** Most annotated peaks shift to two peaks at high electrophoretic mobility upon hexosaminidase treatment. The minor peak represent the non-fucosylated core N-glycan, the major peak represents the fucosylated trimannosyl core N-glycan. **Panel f:** We observe core fucosylation for the majority of the N-glycans. This is illustrated by a shift towards higher electrophoretic mobility of many of the observed peaks after fucosidase treatment of the glycans. **Panel g:** We did not observe any major changes in the glycan profile upon treatment with a broad-spectrum sialidase, suggesting the absence of sialylation in the glycans of GM-CSF produced in 293S cells.

Supplementary Figure 8

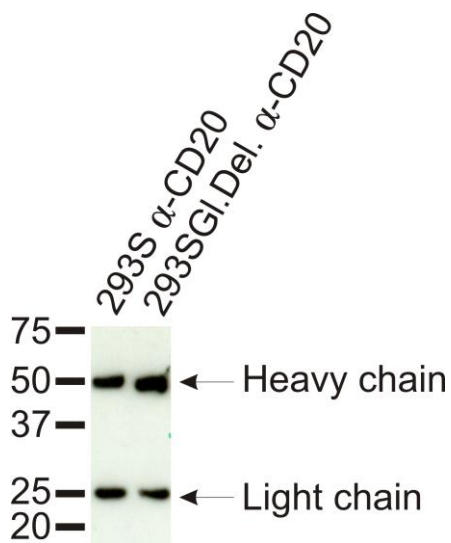
MALDI-TOF-MS analysis of hGM-CSF produced in 293SGlycoDelete and 293S cells.



Supplementary Fig. 11 Panel 1: 293S-produced hGM-CSF. The enormous observed heterogeneity is largely due to the variability of 293S N-glycosylation. **Panel 2:** hGM-CSF sialidase digest results in some heterogeneity reduction. **Panel 3:** hGM-CSF digested with PNGaseF has a strongly reduced heterogeneity, demonstrating that N-glycosylation is the main source of molecular weight heterogeneity. **Panel 4:** 293SGlycoDelete produced hGM-CSF has a strongly reduced heterogeneity. **Panel 5:** Sialidase digest on 293SGlycoDelete produced hGM-CSF reveals a pattern of similarly low complexity as the completely de-N-glycosylated 293S-produced protein.

Supplementary Figure 9

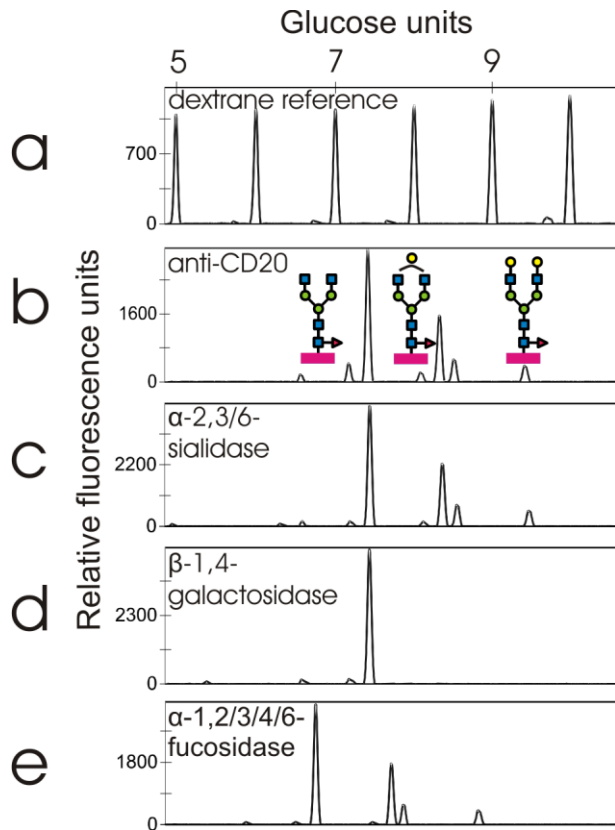
Immunoblot analysis of anti-CD20 produced in 293S or 293SGlycoDelete cells.



Supplementary Fig. 9. Equal volumes of culture medium of 293S wild-type cells and 293SGlycoDelete cells upon transient transfection using identical methods were analysed by immunoblotting. Consequently, the blot shows the level of protein expression of the anti-CD20 monoclonal antibody in the culture medium. The yield of the recombinant protein is similar for both cell lines, indicating that the genetic manipulations used to derive GlycoDelete 293 cells from the WT 293S precursors do not substantially affect the cell's capacity of protein secretion.

Supplementary Figure 10

DSA-FACE analysis of anti-CD20 produced in 293S cells.



Supplementary Fig. 10. Panel a: dextran ladder reference. **Panel b:** DSA-FACE profile of untreated anti-CD20 produced in 293S cells with annotated structures. Glycosylation of anti-CD20 produced in 293S cells results in core-fucosylated diantennary N-glycans with or without galactosylation. **Panel c:** We did not observe any major changes in the glycan profile upon treatment with a broad-spectrum sialidase, suggesting the absence of sialylation in the glycans of anti-CD20 produced in 293S cells. **Panel d:** Galactosylated structures disappear from the spectrum upon galactosidase digestion. A single peak remains, representing the non-galactosylated core-fucosylated diantennary N-glycan. **Panel e:** We observe core fucosylation for all detected N-glycans. This is illustrated by a shift towards higher electrophoretic mobility of the observed peaks after fucosidase treatment of the glycans.

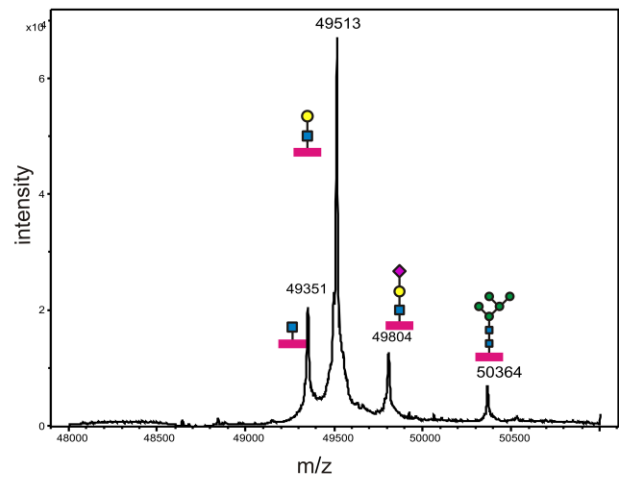
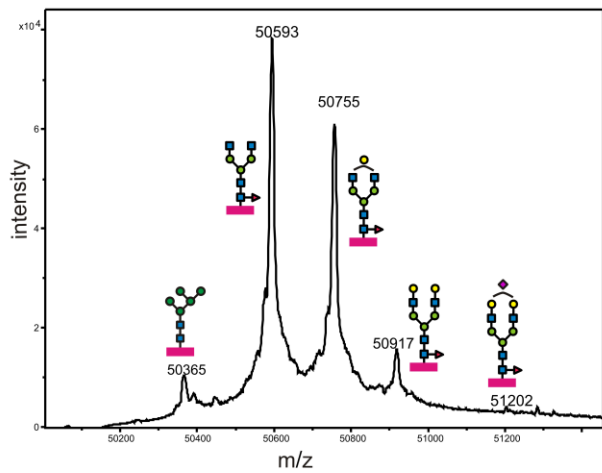
Supplementary Figure 11

LC-MS analysis of anti-CD20 IgG1 produced in 293S (left) and 293SGlycoDelete (right) cells.

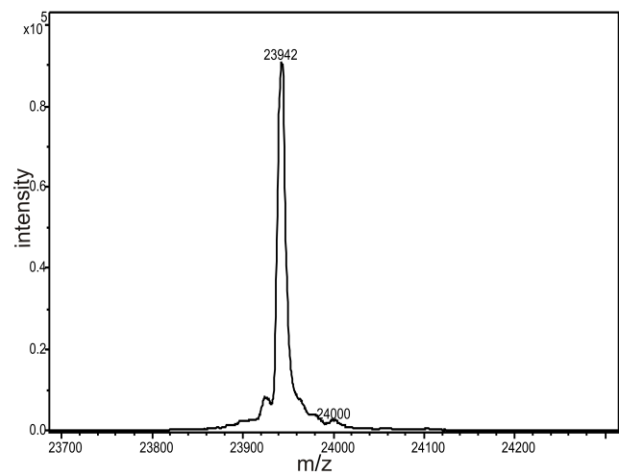
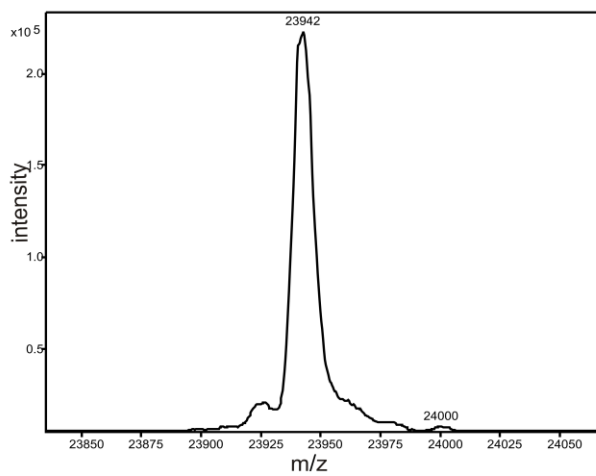
293S anti-CD20

293SGlycoDelete anti-CD20

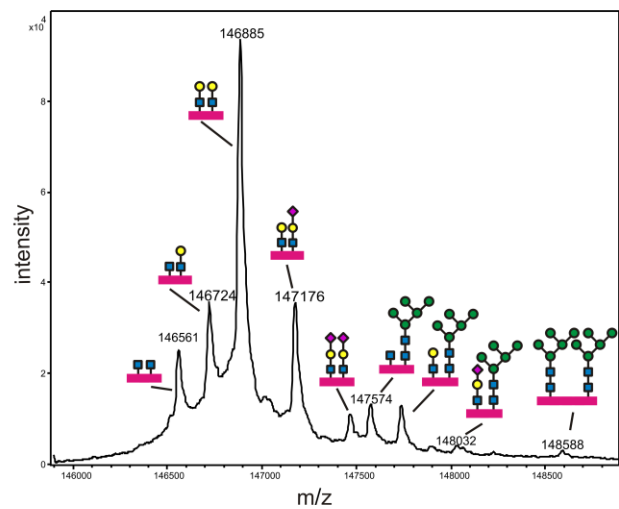
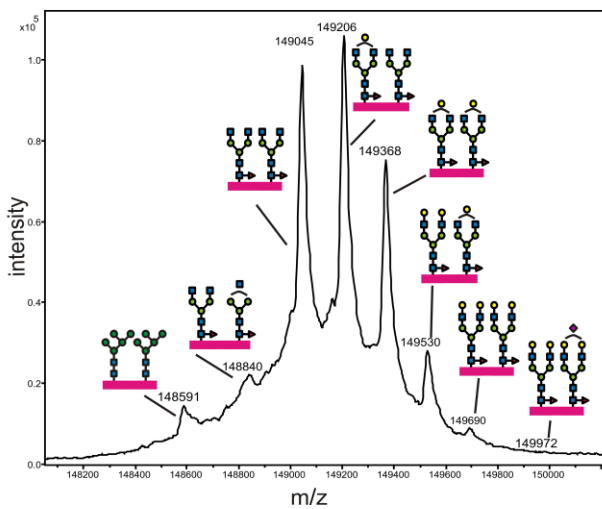
A) Reduced heavy chain



B) Reduced light chain



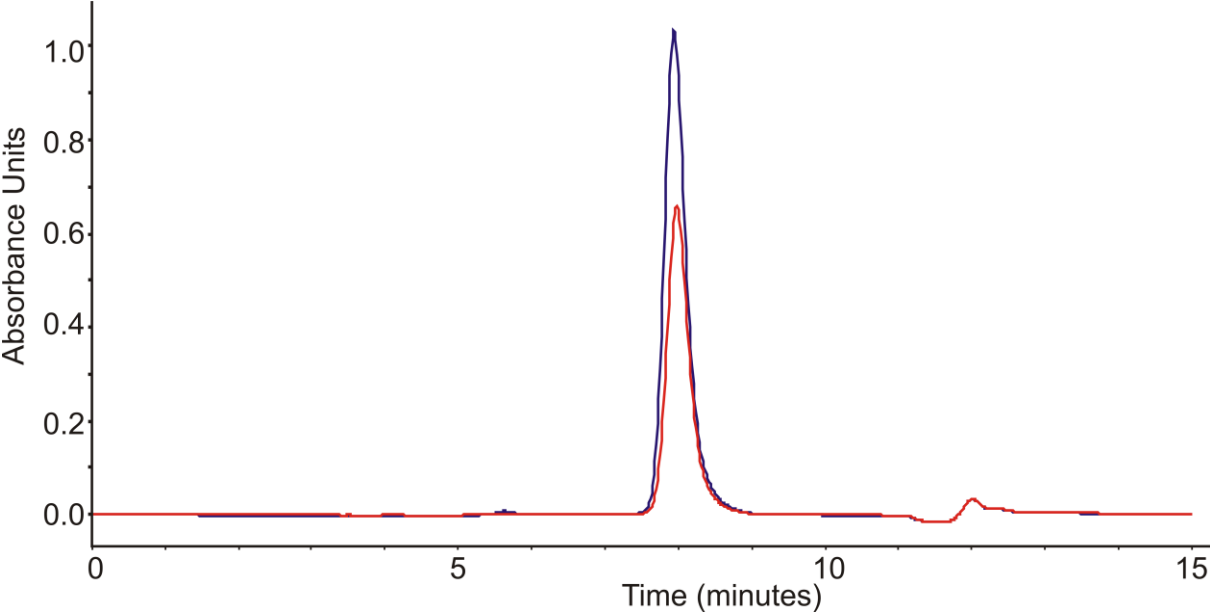
C) Intact antibody



Supplementary Fig. 11 Row A: deconvoluted ESI spectrum for the reduced heavy chain, which carries the single N-glycosylation site. For 293S-produced anti-CD20, the typical core-fucosylated agalacto-, mono-, and bigalactosylated biantennary glycans are the dominant species, while a low amount of Man₅Gn₂ N-glycan is also detected. Sialylation is almost undetectable. For the 293SGlycoDelete anti-CD20, HexNAc-Asn, Hex-HexNAc-Asn and NeuNAc-Hex-HexNAc-Asn dominate the spectrum, while also here a minor fraction of Man₅Gn₂ is formed. Importantly, no non-N-glycosylation related heterogeneity is detectable, supporting the notion that GlycoDelete manipulation of HEK293 cells does not lead to the unexpected induction of other post-translational modification pathways **Row B:** The light chain was unaffected by the GlycoDelete engineering as it carries no N-glycosylation sites. **Row C:** Deconvoluted mass spectra for the intact, non-reduced antibody. All species can be interpreted as a combinatorial series of the glycoforms on both heavy chains. In both antibodies, the number of S-S bridges is calculated as 12-13 based on the difference in mass between the reduced chains and the assembled antibody.

Supplementary Figure 12

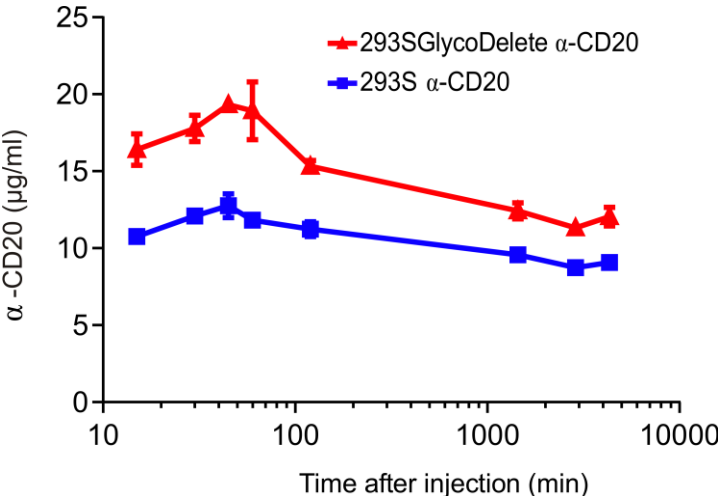
Size exclusion chromatography of anti-CD20



Supplementary Fig. 12. Size exclusion chromatography of 293S anti-CD20 (blue line) and 293SGlycoDelete anti-CD20 (red line). Only the monomeric peak is detected indicating that there is no aggregation in both glycoforms.

Supplementary Figure 13

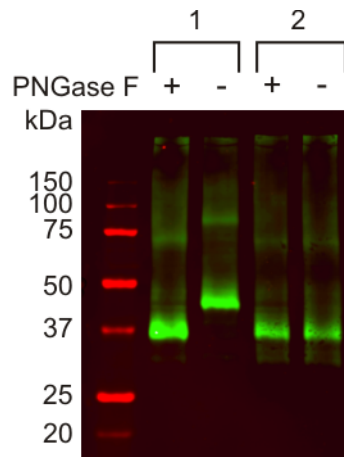
Anti-CD20 pharmacokinetics in mice.



Supplementary Fig. 14. Repeat experiment in an independent laboratory from the experiment shown in Fig. 3 of the main text, also including earlier time points post-injection. Before reaching the peak concentration in the blood, less of the anti-CD20 is removed, resulting in increased circulating levels. The subsequent slow clearance (beyond 1h post-injection) is comparable for both glycoforms, as observed also in the experiment reported in Fig. 3.

Supplementary Figure 14

Immunoblotting of 5HT1DR produced in 293SGnTI^{-/-} and 293SGlycoDelete cells.

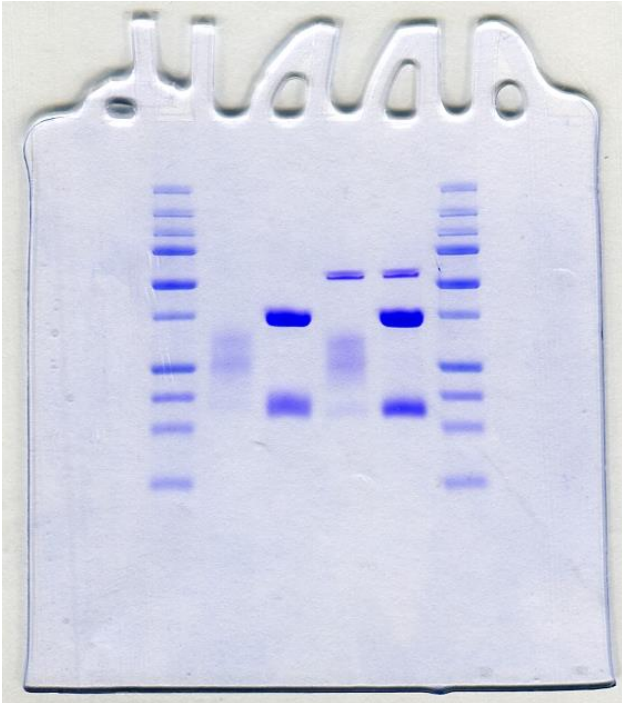


Supplementary Fig. 15. Treatment of membrane protein extracts with PNGaseF revealed a large shift in the molecular weight (MW) of the 5HT1DR stably produced in 293SGnTI^{-/-} cells (1), as expected. Contrary to this, receptor produced in 293SGlycoDelete cells (2) did not shift in MW upon PNGaseF treatment and ran at approximately the same MW as PNGaseF treated receptor from 293SGnTI^{-/-} cells. This is consistent with a complete removal of the 5HT1DR N-glycans in the 293SGlycoDelete cells.

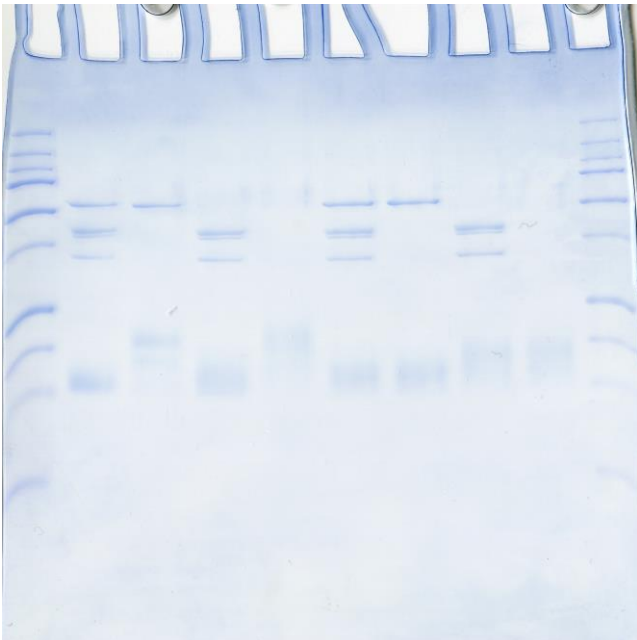
Supplementary Figure 15

Non cropped SDS-PAGE gels from main figures

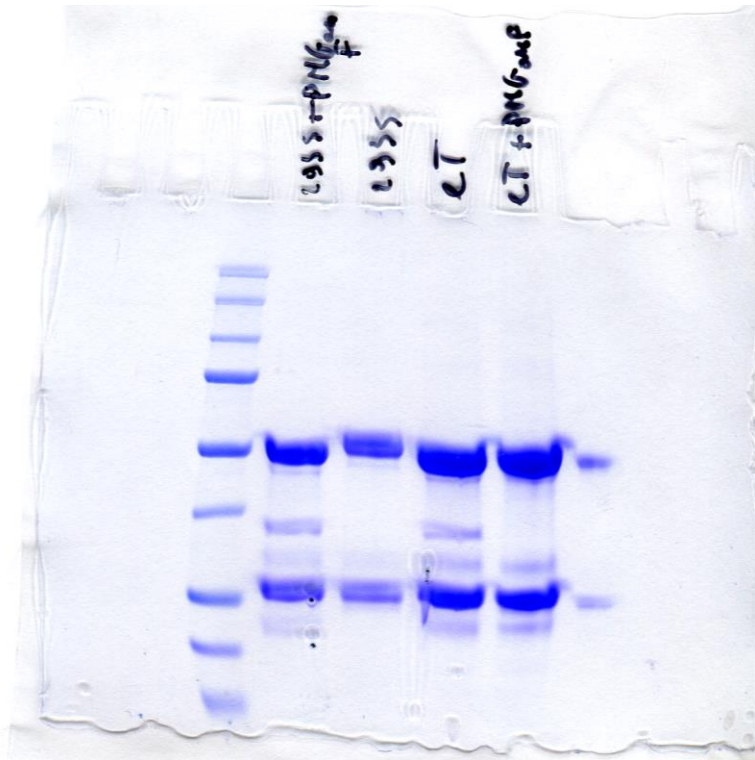
a



b



c



Supplementary Figure 15 Panel a) Non cropped version of Figure 2a left panel. **Panel b)** Non cropped version of Figure 2a middle and right panel. **Panel c)** Non cropped version of figure 3a.

Supplementary table 1

Dissociation constants (K_D) of the Fc binding with hFcRn, mFcRn and Fc γ RIIIaV.

| | GlycoDelete | 293S | K_D fold reduction |
|--------------------|-------------|----------|----------------------|
| hFcRn | 6,72E-09 | 5,60E-09 | 0,83 |
| mFcRn | 2,24E-10 | 2,58E-10 | 1,15 |
| Fc γ RIIIaV | 2.90E-06 | 5.00E-07 | 5,8 |

Supplementary Table 1. Both hFcRn and mFcRn binding was determined with SPR and we found for both glycoforms a K_D within the same range. IgG binding to Fc γ RIIIaV was determined using BLI. 293SGlycoDelete it's K_D is reduced with a factor 5,8 compared to the WT glycoform.

Supplementary table 2

Data underlying figure 1c

| 293SGlycoDelete | | | | | | | |
|-----------------|--------|--------|--------|--------|--------|------------|-------------------|
| hours | Well 1 | Well 2 | Well 3 | Avg | St Dev | Cells/well | Cells/well St dev |
| 0 | 27 | 23 | 21 | 23,67 | 3,06 | 157778 | 20367 |
| 24 | 36 | 37 | 26 | 33,00 | 6,08 | 220000 | 40552 |
| 48 | 53 | 42 | 39 | 44,67 | 7,37 | 297778 | 49141 |
| 72 | 150 | 194 | 208 | 184,00 | 30,27 | 1226667 | 201770 |
| 96 | 270 | 282 | 234 | 262,00 | 24,98 | 1746667 | 166533 |
| 120 | 468 | 510 | 378 | 452,00 | 67,44 | 3013333 | 449592 |
| 144 | 492 | 519 | 465 | 492,00 | 27,00 | 3280000 | 180000 |
| 168 | 549 | 510 | 504 | 521,00 | 24,43 | 3473333 | 162891 |
| 192 | 512 | 476 | 532 | 506,67 | 28,38 | 3377778 | 189189 |
| | | | | | | | |
| | | | | | | | |
| | | | | | | | |
| | | | | | | | |
| 293SGnTI/- | | | | | | | |
| hours | Well 1 | Well 2 | Well 3 | Avg | St Dev | cells/well | Cells/well St dev |
| 0 | 29 | 27 | 23 | 26,33 | 3,06 | 175556 | 20367 |
| 24 | 55 | 58 | 45 | 52,67 | 6,81 | 351111 | 45379 |
| 48 | 51 | 61 | 72 | 61,33 | 10,50 | 408889 | 70026 |
| 72 | 199 | 176 | 168 | 181,00 | 16,09 | 1206667 | 107290 |
| 96 | 266 | 268 | 210 | 248,00 | 32,92 | 1653333 | 219494 |
| 120 | 360 | 404 | 402 | 388,67 | 24,85 | 2591111 | 165641 |
| 144 | 450 | 447 | 468 | 455,00 | 11,36 | 3033333 | 75719 |
| 168 | 501 | 444 | 471 | 472,00 | 28,51 | 3146667 | 190088 |
| 192 | 516 | 464 | 496 | 492,00 | 26,23 | 3280000 | 174865 |

Supplementary table 3

Data underlying figure 2d

| ng/mL | 293S | | | 293 Glycodelete | | | E. Coli | | |
|--------|-------|--------|--------|-----------------|--------|--------|---------|--------|--------|
| 54 | 0,686 | 0,709 | 0,702 | 0,665 | 0,637 | 0,731 | 0,612 | 0,661 | 0,671 |
| 18 | 0,687 | 0,657 | 0,648 | 0,691 | 0,658 | 0,724 | 0,627 | 0,705 | 0,642 |
| 6 | 0,593 | 0,665 | 0,619 | 0,63 | 0,67 | 0,693 | 0,632 | 0,704 | 0,601 |
| 2 | 0,588 | 0,646 | 0,593 | 0,615 | 0,587 | 0,719 | 0,495 | 0,577 | 0,525 |
| 0,6667 | 0,548 | 0,605 | 0,555 | 0,568 | 0,601 | 0,674 | 0,298 | 0,37 | 0,308 |
| 0,2222 | 0,436 | 0,522 | 0,49 | 0,528 | 0,557 | 0,618 | 0,138 | 0,185 | 0,143 |
| 0,0741 | 0,266 | 0,384 | 0,321 | 0,365 | 0,446 | 0,446 | 0,042 | 0,074 | 0,053 |
| 0,0247 | 0,133 | 0,202 | 0,17 | 0,248 | 0,27 | 0,314 | -0,021 | 0,015 | -0,026 |
| 0,008 | 0,048 | 0,076 | 0,068 | 0,142 | 0,132 | 0,156 | -0,056 | -0,042 | -0,069 |
| 0 | -0,07 | -0,088 | -0,082 | -0,057 | -0,102 | -0,059 | -0,081 | -0,084 | -0,101 |

Supplementary table 4

Data underlying figure 2e

| eT sialidase + galactosidase/R2 | eT sialidase/R2 | eT not treated/R ₂ | no protein/R ₂ | eT sialidase + galactosidase/R1 | eT sialidase/R1 | eT not treated/R ₁ | no protein/R ₁ | Antibody dilution | Antibody dilution |
|---------------------------------|-----------------|-------------------------------|---------------------------|---------------------------------|-----------------|-------------------------------|---------------------------|-------------------|-------------------|
| 3,5 | 3,5 | 3,5 | 0,276 | 3,5 | 3,5 | 3,5 | 0,396 | 1 | 1 |
| 3,5 | 3,5 | 3,5 | 0,189 | 3,5 | 3,5 | 3,5 | 0,197 | 2 | 2 |
| 3,5 | 3,5 | 3,5 | 0,16 | 3,5 | 3,5 | 3,5 | 0,187 | 4 | 4 |
| 3,5 | 3,5 | 3,5 | 0,195 | 3,5 | 3,5 | 3,5 | 0,218 | 8 | 8 |
| 3,5 | 3,5 | 3,5 | 0,138 | 3,058 | 3,161 | 3,015 | 0,151 | 16 | 16 |
| 3,225 | 3,279 | 3,15 | 0,126 | 2,307 | 2,326 | 2,198 | 0,16 | 32 | 32 |
| 2,789 | 2,754 | 2,695 | 0,144 | 1,564 | 1,554 | 1,462 | 0,166 | 64 | 64 |
| 1,903 | 1,865 | 1,792 | 0,123 | 0,907 | 0,924 | 0,862 | 0,098 | 128 | 128 |
| 1,192 | 1,201 | 1,13 | 0,147 | 0,57 | 0,538 | 0,533 | 0,107 | 256 | 256 |
| 0,723 | 0,746 | 0,69 | 0,106 | 0,332 | 0,353 | 0,363 | 0,08 | 512 | 512 |
| 0,439 | 0,449 | 0,419 | 0,125 | 0,228 | 0,218 | 0,199 | 0,077 | 1024 | 1024 |
| 0,106 | 0,102 | 0,115 | 0,099 | 0,128 | 0,098 | 0,102 | 0,075 | 2048 | 2048 |

Supplementary table 5

Data underlying figure 3c

| Antibody concentration µg/mL | Anti-CD20 293 | | | Anti-CD20 293 Glycodelete | | |
|---------------------------------|---------------|--------|--------|---------------------------|--------|--------|
| | | | | | | |
| 10 | 2637,7 | 2563,4 | 2582,8 | 2633,8 | 2599,3 | 2539,1 |
| 2,5 | 2145,8 | 2177,3 | 1924,2 | 2223,5 | 2130,6 | 2250,8 |
| 0,625 | 1501,8 | 1516,7 | 1548,3 | 1434,7 | 1511,1 | 1554,9 |
| 0,15625 | 673,3 | 673,1 | 644 | 602,4 | 662,6 | 667,1 |
| 0,039063 | 240,9 | 234 | 210,2 | 206,7 | 216,2 | 248,7 |
| 0,009766 | 76,4 | 79,7 | 72,2 | 71,5 | 68,2 | 75,9 |
| 0,002441 | 28,6 | 27,5 | 23,2 | 26,8 | 24,6 | 26,9 |
| 0,00061 | 14,1 | 12,3 | 11,3 | 14 | 10 | 19 |

Supplementary table 6

Data underlying figure 3e

FcγRI

| Ab Concentration μg/ml | Glycodelete Anti CD20 | | | 293 Anti CD20 | | |
|---------------------------|-----------------------|-------|-------|---------------|-------|-------|
| | 50 | 0,315 | 0,324 | 0,317 | 0,085 | 0,091 |
| 10 | 1,163 | 1,153 | 1,143 | 0,143 | 0,143 | 0,141 |
| 2 | 2,418 | 2,324 | 2,324 | 0,388 | 0,379 | 0,377 |
| 0,4 | 3,079 | 2,886 | 2,961 | 1,138 | 1,105 | 1,102 |
| 0,08 | 3,215 | 3,165 | 3,257 | 2,243 | 2,198 | 2,332 |
| 0,016 | 3,389 | 3,339 | 3,387 | 3,049 | 3,036 | 3,156 |
| 0,0032 | 3,379 | 3,443 | 3,344 | 3,394 | 3,397 | 3,437 |
| 0,0006 | 3,474 | 3,589 | 3,506 | 3,428 | 3,598 | 3,602 |

FcγRIIa

| Antibody Concentration μg/ml | Anti-CD20 293 Glycodelete | | | Anti-CD20 293 | | |
|---------------------------------|---------------------------|-------|-------|---------------|-------|-------|
| | 2,69897 | 1,559 | 2,638 | 2,573 | 0,684 | 0,732 |
| 2,22185 | 2,408 | 2,7 | 2,761 | 1,502 | 1,644 | 1,682 |
| 1,744731 | 2,182 | 2,905 | 2,918 | 2,113 | 2,463 | 2,359 |
| 1,267617 | 2,529 | 3,021 | 3,014 | 2,433 | 2,907 | 2,725 |
| 0,790496 | 2,389 | 2,967 | 3,191 | 2,564 | 2,907 | 2,981 |
| 0,313445 | 2,521 | 3,019 | 3,103 | 2,569 | 2,965 | 2,932 |
| -0,16368 | 2,441 | 2,944 | 3,068 | 2,687 | 3,023 | 3,099 |
| -0,64016 | 2,438 | 3,058 | 3,031 | 2,605 | 2,885 | 2,98 |

FcyRIIb

| Antibody Concentration µg/ml | Anti-CD20 293 Glycodelete | | Anti-CD20 293 | |
|---------------------------------|------------------------------|-------|---------------|-------|
| | | | | |
| 2300 | 0,962 | 0,84 | | |
| 766,67 | 1,476 | 1,356 | | |
| 255,56 | 1,56 | 1,62 | | |
| 85,19 | 1,769 | 1,678 | | |
| 28,4 | 1,739 | 1,73 | | |
| 9,47 | 1,871 | 1,814 | | |
| 3,16 | 1,899 | 1,827 | | |
| 3000 | | | 0,284 | 0,274 |
| 1000 | | | 0,641 | 0,629 |
| 333,33 | | | 1,061 | 1,098 |
| 111,11 | | | 1,517 | 1,49 |
| 37,04 | | | 1,662 | 1,545 |
| 12,35 | | | 1,991 | 1,874 |
| 4,12 | | | 2,268 | 1,918 |

ADCC

| Antibody Concentration µg/mL | Anti-CD20 293 Glycodelete | | Anti-CD20 293 | |
|---------------------------------|------------------------------|-------|---------------|-------|
| | | | | |
| 2,3 | 52,44 | 50,35 | | |
| 0,46 | 46,6 | 48,82 | | |
| 0,092 | 42,04 | 45,15 | | |
| 0,0184 | 33,85 | 32,4 | | |
| 0,00368 | 16,5 | 15,22 | | |
| 0,000736 | 4,52 | 4,43 | | |
| 0,000147 | 0,26 | -1,11 | | |
| 2,94E-05 | 1,66 | -0,17 | | |
| 3 | | | 52,14 | 56,15 |
| 0,6 | | | 53,29 | 49,37 |
| 0,12 | | | 51,84 | 51,42 |
| 0,024 | | | 51,76 | 49,07 |
| 0,0048 | | | 43,7 | 44,64 |
| 0,00096 | | | 21,62 | 21,36 |
| 0,000192 | | | 4,26 | 8,44 |
| 3,84E-05 | | | 2,26 | 1,45 |

Supplementary table 7

Data underlying figure 3f

| 293SGlycoDelete a- CD20 + galactosidase + sialidase | 293SGlycoDelete a- CD20 + sialidase | | | 293SGlycoDelete a- CD20 | | | No protein | | | Antibody dilution | | | |
|---|--|-------|-------|----------------------------|-------|-------|------------|-------|-------|-------------------|-------|-------|--------|
| | 3,5 | 3,43 | 3,5 | 3,5 | 3,5 | 3,5 | 3,5 | 3,428 | 3,5 | | 0,459 | 0,458 | 0,484 |
| 3,5 | 3,5 | 3,5 | 3,5 | 3,5 | 3,5 | 3,5 | 3,5 | 3,5 | 3,5 | 0,179 | 0,161 | 0,162 | 150 |
| 3,231 | 3,147 | 3,212 | 3,16 | 3,398 | 3,335 | 3,252 | 3,283 | 3,25 | 3,25 | 0,077 | 0,081 | 0,019 | 450 |
| 2,778 | 2,628 | 2,851 | 2,815 | 2,879 | 2,864 | 2,798 | 2,689 | 2,906 | 2,906 | 0,054 | 0,068 | 0,025 | 1350 |
| 1,902 | 1,756 | 1,914 | 1,992 | 2,159 | 2,387 | 1,982 | 1,968 | 2,043 | 2,043 | 0,034 | 0,043 | 0,016 | 4050 |
| 1,048 | 0,931 | 1,024 | 1,09 | 1,281 | 1,308 | 1,07 | 1,045 | 1,188 | 1,188 | 0,02 | 0,049 | 0,013 | 12150 |
| 0,477 | 0,494 | 0,456 | 0,524 | 0,48 | 0,619 | 0,5 | 0,513 | 0,278 | 0,278 | 0,023 | 0,046 | 0,061 | 36450 |
| 0,225 | 0,211 | 0,198 | 0,232 | 0,215 | 0,274 | 0,216 | 0,21 | 0,207 | 0,207 | 0,02 | 0,037 | 0,002 | 109350 |
| 0,121 | 0,103 | 0,085 | 0,116 | 0,1 | 0,186 | 0,109 | 0,138 | 0,081 | 0,081 | 0,02 | 0,021 | 0,001 | 328050 |
| 0,083 | 0,074 | 0,043 | 0,07 | 0,06 | 0,051 | 0,073 | 0,053 | 0,035 | 0,035 | 0,018 | 0,03 | 0,005 | 984150 |

Supplementary table 8

Data underlying figure 3g

| Time (h) | Anti-CD20 293s | | | | Anti-CD20 293GlycoDelete | | | |
|----------|----------------|----------|----------|----------|--------------------------|----------|----------|----------|
| 1 | 16,1974 | 13,17261 | 17,00356 | 11,66813 | 28,8332 | 29,3877 | 33,474 | 36,6924 |
| 24 | 7,4006 | 9,311962 | 8,466237 | 6,55145 | 14,78954 | 16,3589 | 14,10662 | 13,68416 |
| 48 | 7,21618 | 7,227962 | 6,746963 | 7,31205 | 19,8775 | 13,93023 | 15,7465 | 17,25974 |
| 96 | 6,76923 | 8,425325 | 6,122825 | 7,1901 | 12,1798 | 14,31522 | 17,8752 | 14,34155 |
| 168 | 5,17352 | 7,374187 | 5,897713 | 6,8257 | 11,631 | 14,21366 | 11,92079 | 11,60133 |
| 240 | 4,16867 | 3,625075 | 5,712138 | 6,59155 | 11,51135 | 11,86461 | 10,81969 | 11,3477 |
| 336 | 3,88537 | 4,81935 | 4,346875 | 2,606795 | 7,239687 | 10,82754 | 7,92285 | 7,9431 |
| 504 | 3,13270 | 2,52692 | 2,639255 | 2,566235 | 5,357775 | 6,811675 | 5,078675 | 5,5248 |
| 672 | 1,59795 | 1,916417 | 1,99827 | 1,65403 | 3,349695 | 3,54475 | 3,661225 | 3,075095 |

Supplementary Methods

Methods Supplementary Figure 1:

Construction of pCAGGS-s-endoT, pCAGGS-GM₂S-endoT and pCAGGS-ST-endoT. The endoT coding sequence³ without the signal sequence was amplified from a pUC19 cloning vector containing the full size endoT coding sequence, with PCR primers PR1 and PR4 (for ST-endoT), PR2 and PR4 (for GM₂S-endoT) or PR3 and PR4 (for 'endoT'). All primer sequences are provided in Supplementary Note 2. The coding sequence for the N-terminal parts of ST6GalI⁴ (for ST-endoT) and B4GALNTI⁵ (for GM₂S-endoT) was amplified from a human hepatoma G2 cDNA library with primers PR5, PR6 and PR7, PR8 respectively. Fusion PCR reactions to generate the ST-endoT, the GM₂S-endoT and endoT without signal sequence were set up using PR5 and PR4, PR7 and PR4 and PR3 and PR4 respectively. Subsequent digestion of the fusion PCR products ST-endoT, GM₂S-endoT and endoT with XhoI and Bsu36I and ligation into an XhoI and Bsu36I digested and dephosphorylated pCAGGS plasmid, resulted in the pCAGGS-ST-endoT and pCAGGS-GM₂S-endoT plasmids. The dsDNA signal sequence for the s-endoT construct was produced by annealing oligonucleotides PR9 and PR10. The pCAGGS-endoT plasmid was digested with XhoI and KpnI. Subsequent ligation of the adapter into the plasmid resulted in the pCAGGS-s-endoT plasmid.

Transfection and sample preparation. Cells were transfected as described (see online methods). 3 days post transfection with pCAGGS-s-endoT, pCAGGS-GM₂S-endoT or pCAGGS-ST-endoT, cells and supernatants were harvested. For cell lysates, cells were collected by centrifugation at 1000 rpm and washed once with PBS. Cell lysates were prepared by incubating ~1 million cells with 500 µl RIPA buffer (150 mM sodium chloride, 1.0% Igepal CA-630, 0.5% sodium deoxycholate, 0.1% sodium dodecyl sulphate and 50 mM Tris, pH 8.0) at 4°C on a rotating platform for 30 minutes, followed by centrifugation at 14,000 rpm for 10 minutes and discarding the insoluble material. 20 µl samples were supplemented with 5 µl 5x SDS-PAGE loading buffer (8.3 % SDS, 41.7 % glycerol, 0.1 % bromophenol blue, 208 mM Tris-HCl, pH 6.8 and 65 mM dithiothreitol added fresh) and boiled for 10 minutes.

500 µl samples of cell culture supernatants were cleared by centrifugation for 10 minutes at 14,000 rpm in a microcentrifuge, acetone precipitated by adding 2 volumes of ice cold acetone and incubated on ice for 30 minutes. Precipitated samples were centrifuged for 10 minutes at 14,000 rpm in a microcentrifuge and the supernatants were discarded. Pellets were dissolved by adding 80 µl of ultrapure water and 20 µl 5x SDS-PAGE loading buffer, followed by boiling to dissolve and denature protein pellets.

Immunoblotting. 25 µl aliquots of cell lysates or supernatant samples were analysed for the presence of endoT fusion proteins by immunoblotting. Indirect detection was performed using a custom generated rabbit polyclonal antibody against the endoT enzyme (CER groupe, Département Santé, Marloie, Belgium) diluted 1/5,000. The antigen to generate the custom rabbit polyclonal was endoT produced in *Pichia pastoris* and purified previously in our lab.

The injected antigen preparation was 1 mg/ml antigen in phosphate buffered saline. The secondary antibody was an IRDye 680 goat anti rabbit IgG (catalog number 926-68021, LI-COR Biosciences, Lincoln, NE, USA). To assess C-terminal processing, the same blots were probed with a mouse primary antibody directed against the myc tag (catalog number AHO0062, Life Technologies, Paisley, UK) and an IRDye 800 goat anti mouse IgG secondary antibody (catalog number 926-32210, LI-COR Biosciences, Lincoln, NE, USA).

Methods Supplementary Figure 2:

To evaluate the *in vivo* de-N-glycosylation by the endoT fusion proteins, the fusion constructs were transiently transfected (transfection, see Online Methods) to 293SGnTI^{-/-} cells that stably and inducibly expressed the Flt3 receptor extracellular domain (Flt3ECD), C-terminally tagged with a penta-His tag (cells kindly provided by Prof. Dr. S. Savvides, Ghent University). The producer cell lines were transfected with the endoT fusion constructs or empty plasmid and induced with 2 µg/ml tissue culture grade tetracycline and 5 mM sodium butyrate (both Sigma-Aldrich, St. Louis, MO, USA). Supernatants (for Flt3ECD production) were harvested 48 hours and 72 hours post transfection/induction.

For the Flt3ECD, 20 µl aliquots of cell supernatants were run on SDS-PAGE and the processing of the Flt3 was analysed by western blotting. The primary antibody was a mouse Penta-his antibody (Catalog number 34660, Qiagen, Hilden, Germany) and the secondary antibody an anti-mouse IgG-coupled to HRP (Catalog number NA931, GE Healthcare Biosciences, Pittsburgh, PA, USA).

Methods Supplementary Figure 3:

Early passages of both of the endoT-expressing clones (#+8) and 293SGnTI^{-/-} cells were plated in 24-well plates at 30,000 cells per well in the presence of increasing ConA concentrations: 0 – 20 µg/ml. ConA was added immediately upon passaging. We assessed at which concentration ConA had reduced the growth of the different lines to less than 10% confluence of the well.

Methods Supplementary Figure 4:

EndoT construct genomic integration validation. To validate the presence of the CDS, genomic DNA was prepared from ~1 million cells of both the 293SGlycoDelete and 293SGnTI^{-/-} cell lines with the Gentra Puregene Core kit A (Qiagen, Hilden, Germany), according to the manufacturer's instructions. A touchdown PCR reaction was performed with the Phusion[®] High-Fidelity DNA polymerase (New England Biolabs, Ipswich, MA, USA) employing ~10 ng genomic DNA for each 50 µl reaction and primers PR11 and PR12. PCR cycling was a touchdown protocol with the primer annealing temperature lowered by 1°C every two cycles, from 67°C to 64°C and held at 64°C for 30 cycles (accounting for 36 cycles in total). PCR products were analysed with a Shimadzu MultiNA microchip DNA/RNA electrophoresis system, employing the DNA-500 reagent kit (Shimadzu Corporation, Kyoto, Japan) according to the manufacturer's instructions.

EndoT fusion protein expression validation. The expression of the ST-endoT protein was assessed by western blotting. Methods are the same as described for Supplementary Fig. 1, except that the secondary antibody was an IRDye 800 Goat anti rabbit IgG antibody (Catalog number 926-32211, LI-COR Biosciences, Lincoln, NE, USA).

Methods Supplementary Figure 5:

Differential gene expression analysis. The methods for this Supplementary Figure are the same as for Figure 1d (Supplementary Note 2).

Methods Supplementary Figure 6:

Sample preparation for MALDI mass spectrometry. The methods for this Supplementary Figure are the same as described in online methods and Supplementary Note 4.

Methods Supplementary Figure 7:

DSA-FACE analysis of 293S GM-CSF. N-linked oligosaccharides were prepared from purified proteins upon blotting to PVDF membrane in the wells of 96-well plate membrane plates, and were analyzed by capillary electrophoresis with laser-induced fluorescence detection (CE-LIF) using an ABI 3130 capillary DNA sequencer as described previously⁶.

Methods Supplementary Figure 8:

MALDI-TOF MS for intact GM-CSF. We diluted 5 µg of 293S GM-CSF or 293SGlycoDelete GM-CSF to a total volume of 20 µL with 50 mM phosphate buffer pH 7.0. Either no enzyme, 20 mU of *Arthrobacter ureafaciens* sialidase or 100 U of PNGase F (both in house production) was added. The samples were incubated overnight at 37°C. The following morning, the samples were cleaned up and desalted with C4 ZipTip® pipette tips (Millipore, Billerica, MA, USA) according to the manufacturer's instructions. The samples were eluted in 5 µl 50% ACN/water + 0.1% trifluoro acetic acid (Sigma-Aldich). 1 µl aliquots of the samples were spotted on a MALDI target plate with 1 µl 20 mg/ml alpha-cyano-4-hydroxycinnamic acid (CHCA) and analysed on an Applied Biosystems 4800 proteomics analyzer in the linear mode with a laser energy of 5800 and a delayed extraction time of 2000.

Methods Supplementary Figure 9:

Immunoblot analysis of anti-CD20 expression in crude cell supernatant. 20 µl aliquots of fresh cell culture medium were analysed for the presence of anti-CD20 by western blotting. Anti-CD20 was detected using an HRP-labeled anti-human IgG F(ab')₂ antibody (Catalog number AQ112P, Millipore, Billerica, MA, USA) diluted 1/5,000.

Methods Supplementary Figure 10:

DSA-FACE analysis of 293S anti-CD20. The methods for this Supplementary Figure are the same as for Supplementary Figure 7.

Methods Supplementary Figure 11:

LC-MS of intact anti-CD20:

The sample was diluted to 1.0 mg/mL using 50 mM Tris pH 7.5. Subsequently, 10 µL (10 µg) of antibody solution was injected onto a POROS R2/10 2.1x30 mm column (Applied Biosystems) and eluted using a gradient of 0.05% TFA in Milli Q and 0.05% TFA in ACN delivered by an HP1100 (Agilent Technologies) coupled to a high-resolution ESI-QTOF (Bruker MaXis).

LC-MS of reduced anti-CD20:

50 µg of antibody was reduced in 6 M guanidine-HCl, 50 mM Tris pH 8.0, 20 mM DTT for 20 minutes at 56°C. Subsequently, 10 µL (5 µg) of reduced antibody was injected onto a Zorbax 300Sb-C8 (2.1x150 mm) column (Agilent Technologies) and eluted using a gradient of 0.05% TFA in Milli Q and 0.05% TFA in ACN delivered by an HP1100 (Agilent Technologies) coupled to a high-resolution ESI-QTOF (Bruker MaXis).

Methods Supplementary Figure 12:

Size exclusion chromatography of anti-CD20. Analysis was carried out using a TSKgel G3000SWxl column (Tosoh Bioscience, Stuttgart, Germany) on a Waters HPLC system (Waters 2695, Waters Cooperation, MA, USA) with 200 mM sodium phosphate pH 7.0 as the mobile phase. 100 µl of a 1 µg/µl antibody dilution was injected.

Methods Supplementary Figure 13:

Analysis of anti-CD20 binding affinity to hFcRn and FcγRIII. Experiments with hFcRn were performed as described in the online methods section (SPR experiments). Experiments with FcγRIII were performed as described in the online methods section (BLI experiments).

Methods Supplementary Figure 14:

Pharmacokinetics of the two anti-CD20 glycoforms. Two groups of 40 female, 8 weeks old C57BL/6J mice were purchased (Charles River, MA, USA) and randomly assigned to be intravenously injected with 19,2 µg (1 mg/kg) of either 293S or 293SGlycoDelete anti-CD20. At each time point (15 min, 30 min, 45 min, 1h, 2h, 24h, 48h and 72h), 5 mice per treatment group were sacrificed for a final bleeding and the concentration of anti-CD20 was determined with the FastELISA human IgG kit (RD-Biotech, Besançon, France) according to the manufacturer's instructions. The data points shown in Figure 3g are the mean values (4 mice) for each time point. The error bars are S.E.M. For practical reasons, the investigators were not blinded to the treatment group assignment of the mice. This experiment was approved by the local ethical committees.

Methods Supplementary Figure 15:

Construction of the pT-REx-5HT1DRho-IRESdsRed2 plasmid. The pT-REx-DEST30 plasmid (Invitrogen) was amplified in a dam/dcm methylation deficient *E. coli* strain and digested with BclI and XbaI. A dsDNA insert was created by annealing oligos PR11 and PR12. Subsequent ligation of the dsDNA insert into the XbaI/BclI digested pT-REx-DEST30 fragment generated the pT-REx-MCS plasmid.

We amplified the CDS for the 5-hydroxy tryptamine 1D receptor (NM_00864) from a human fetal brain cDNA library using primers PR13 and PR14 and cloned it into a pCR[®]II-TOPO[®] plasmid (Invitrogen), generating the Topo-5HT1D plasmid. A Rho1D4-tagged 5HT1DR fragment was amplified from the Topo-5HT1D plasmid with primers PR 13 and PR15. We digested the PCR fragment with Sall and the pT-REx-MCS plasmid with PmeI and Sall, followed by dephosphorylation. We ligated these fragments to result in the pT-REx-5HT1DRho plasmid.

We amplified the IRESdsRed2 fragment from the pLV-tTR/KRAB-Red plasmid (a kind gift of Prof. Peter Vandenabeele, VIB-UGent) with primers PR16 and PR17. The pT-REx-5HT1DRho plasmid was digested with PmeI and used with the IRESdsRed2 fragment in a cloneEZ (GenScript USA Inc., NJ, USA) reaction. This resulted in the pT-REx-5HT1DRho-IRESdsRed2 plasmid.

5HT1DR expressing 293SGnTI^{-/-} and 293SGlycoDelete clones. We generated cell lines stably and inducibly expressing the 5HT1D receptor by transfecting 293SGnTI^{-/-} and 293SGlycoDelete cells with the pT-REx-5HT1DRho-IRESdsRed2 plasmid. Selection was performed with G418 (Sigma-Aldrich) at 600 µg/ml (293SGnTI^{-/-} cells) and at 150 µg/ml G418 (293SGlycoDelete cells). We then subjected the G418 resistant cells to limiting dilution cloning in conditioned medium. We induced expression of the 5HT1D receptor with 2 µg/ml tetracyclin and 1 mM valproate (Sigma-Aldrich). We selected the 293SGnTI^{-/-} and 293SGlycoDelete 5HT1DR clones expressing the highest intensity of red fluorescence after 2-3 days of induction by fluorescence microscopy. 5HT1DR expression in the selected clones was validated by ELISA (data not shown).

5HT1D receptor expression and sample preparation. We generated 293SGnTI^{-/-} and 293SGlycoDelete cell lines stably and inducibly expressing the 5HT1D receptor. Detailed methods for the generation of 5HT1DR expression constructs and subsequent generation of stable 5HT1DR-expressing clones are described in the methods of the supplementary figures. The selected 5HT1DR-expressing clone of each line was induced with 2 µg/ml tetracyclin and 1 mM valproate. 3 days post-induction, cells were collected. Cell pellets were resuspended in 5 ml of 20 mM Tris-HCl pH 8.0 + 1 mM EDTA + Complete EDTA-free protease inhibitors (Roche, Mannheim, Germany). 1.25 ml of each sample was sonicated on ice (15 cycles, each cycle: 1 s on and 5 s off, at 20% amplitude) with a VCX500 sonicator (Sonics & Materials Inc., Newtown, CT, USA). We centrifuged the lysates immediately for 10 minutes at 13,000 rpm and 4°C and solubilised the pellets in the buffer described above + 0.35 mM NaCl and 0.5 % n-dodecyl-β-D-maltoside. Debris was removed by immediately centrifuging samples again for 10 minutes at 13,000 rpm at 4°C.

To assess the presence of PNGaseF sensitive N-glycans on the 5HT1D receptor, 50 µl aliquots of the samples, supplemented with 1 % Igepal CA-630 and 200 U of PNGaseF (in house production), or no enzyme, were incubated overnight at 37°C. The samples were analysed by immunoblotting using a mouse anti-rho1D4 primary antibody⁷ (University of British Columbia, Vancouver, Canada), diluted 1/250.

Supplementary Note 1: Primer sequences

| Oligo | Sequence |
|-------|--|
| PR1 | 5'-AACAGGACGTACCCGTTAAAGAACTGCA-3' |
| PR2 | 5'-CGCGAGCACCGTACCCGTTAAAGAACTGCA-3' |
| PR3 | 5'-CTCGAGATGGTACCCGTTAAAGAACTCXAGTTGAGAGC-3' |
| PR4 | 5'-GCACCTGAGGTTACAGATCTTCTTCAGAAATAAGCTTTTGTTCAGCGTTAACCATAGCGTAGTAGTTGATGG-3' |
| PR5 | 5'-GCACTCGAGATGATTCACACCAACCTGAAGA-3' |
| PR6 | 5'-TTAACGGGTACGTCCTTGTCCACACCTG-3' |
| PR7 | 5'-GCACTCGAGATGTGGCTGGGCCGCGGG-3' |
| PR8 | 5'-TTAACGGGTACGGTGCTCGCGTACAGGAGCC-3' |
| PR9 | 5'-TCGAGATGAAGACTATCATTGCTTTGAGCTACATTTCTGTCTGGTTGGGCCCAAGACGTAC-3' |
| PR10 | 5'-GTCTTGGGCCAAACCAGACAGAAAATGTAGCTCAAAGCAATGATAGTCTTCATC-3' |
| PR11 | 5'-GTGCTGCTCCTGGTCTTTC-3' |
| PR12 | 5'-TCAGCCATAGAACCGAAACC-3' |
| PR13 | 5'-CTAGAATTCGCGATATCCCGGGCCAGCGCTGCGGCCGCTCGAGCTAGCGTTTAAACT-3' |
| PR14 | 5'-GATCAGTTTAAACGCTAGCTCGAGCGGCCGAGCGCTGGGCCCGGGATATCGCGAATT-3' |
| PR15 | 5'-GCAGTCGACCATGTCCCACTGAACCACTCAGC-3' |
| PR16 | 5'-GCAGCGGCCGCGGAGGCCTCCGGAAAGGGAC-3' |
| PR17 | 5'-AAACTTAGCGGGAGCCACCTGGCTGCTCAGTACTGGCCTCCGGAAAGGGAC-3' |
| PR18 | 5'-CTCCCGCTAAGTTTAAACGTTTAAACCGGGTAAATTCCGC-3' |
| PR19 | 5'-GATTATGATCAGTTTAAACACTAGTAAATTCTAGAGTCGCGGC-3' |
| PR20 | 5'-CTCAAGGGCCCCTTGACC-3' |
| PR21 | 5'-CGAGCAGAATTCAATGGTGATGATGGTGATGCTCCTGGACTGGCTCCAG-3' |

Supplementary Note 2: Methods gene expression analysis

Total RNA was extracted from 3 replicate cultures of both lines with the RNeasy Midi kit (Qiagen), according to the manufacturer's instructions. RNA quality was assessed on a 2100 Bioanalyzer using RNA 6000 Pico chips (Agilent Technologies, Santa Clara, CA, USA). All samples had an RNA Integrity Number (RIN) of 9.5 or better. After spiking the total RNA samples (RNA sample preparation, see Online Methods) with bacterial poly-A RNA positive controls (Affymetrix, Santa Clara, CA, USA), every sample was reverse transcribed, converted to double-stranded cDNA, *in vitro* transcribed and amplified using the Ambion WT Expression Kit. The obtained single-stranded cDNA was biotinylated after fragmentation with

the WT Terminal Labeling kit (Affymetrix), according to the manufacturer's instructions. The resulting samples were mixed with hybridization controls (Affymetrix) and hybridized on GeneChip Human Exon 1.0 ST Arrays (Affymetrix). The arrays were stained and washed in a GeneChip Fluidics Station 450 (Affymetrix), and scanned for raw probe signal intensities with the GeneChip Scanner 3000 (Affymetrix). Exon array data are MIAME compliant and available from the ArrayExpress database (www.ebi.ac.uk/arrayexpress) under accession number E-MEXP-3516.

We used a combination of the R Statistical Software Package (www.r-project.org) and Affymetrix Power Tools (APT; Affymetrix) for the quality control and differential expression analysis of the exon array data, partly as described earlier⁸. Briefly, exon- and gene-level intensity estimates were generated by background correction, normalization and probe summarization using the Robust Multi-array Average (RMA) algorithm with APT. Quality control of the data before and after normalization was performed in R through the generation of various plots such as box and density plots. Genes of which the expression was undetected in both lines were excluded from further analysis. We considered a gene to be detected when more than half of its exons were detected above the background ($p < 0.05$) in at least 2 of the 3 biological replicates of that cell line. Genes of which the expression was below the estimated noise level in both lines were also removed from further analysis. The noise level threshold was set at a signal intensity level of 8 (the APT output intensity, averaged over the 3 replicates), which eliminated 'detection' of expression of more than 95% of the genes on the Y-chromosome, which is absent from the 293 lineage (which was derived from a female embryo) and thus serves as an appropriate internal negative control.

Differential gene expression analysis was performed using a linear model fit implemented in the R Bioconductor package Limma⁹, considering only core probesets.

Although many statistical assumptions (like normal distribution) for p-value determinations via model-based methods cannot be exactly ascertained for microarray data, it has been argued that p-values remain useful for ranking of genes, even in the presence of large deviations from the assumptions^{10,11}. The Benjamini-Hochberg (BH) method was applied to correct for multiple testing as it was shown to be robust to many forms of dependence between genes even though it assumes independence¹².

Supplementary Note 3: Plasmid construction and protein purification

Construction of the pORF-hGM-CSF-6xHis plasmid. A partial CDS of the human GM-CSF C-terminally tagged with 6 His residues was amplified with primers PR18 and PR19 from the pORF-hGM-CSF plasmid (Invivogen, CA, USA). We digested the PCR fragment and the pORF-hGM-CSF plasmid with Apal and EcoRI and ligated both fragments to result in the pORF-hGM-CSF-6xHis plasmid.

Human GM-CSF purification. 293SGnTI^{-/-} and 293SGlycoDelete cells were transiently transfected with the pORF-hGM-CSF-6xHis plasmid (transient transfection, see online methods). 4 days post transfection, 50 ml of medium containing the expressed protein was

harvested and dialysed against buffer A (20 mM NaH₂PO₄, 0.5 M NaCl and 20 mM imidazole pH 7.5) using 3 kDa molecular weight cut-off membranes. The dialysate was loaded onto a 1 ml His-Trap HP column charged with Ni²⁺ ions (GE healthcare UK Ltd, Buckinghamshire, UK). Then, the column was washed with buffer A until the A₂₈₀ had dropped back to the baseline. After washing the column with 10 column volumes 6 % buffer B (20 mM NaH₂PO₄ pH 7.50 + 20 mM NaCl + 0.5 M imidazole), bound proteins were eluted with 100 % buffer B and collected in 1 ml fractions. The presence of GM-CSF in the collected fractions was verified by tricine SDS-PAGE gel electrophoresis¹³. We measured the protein concentration based on the A₂₈₀ absorbance of the GM-CSF containing fractions versus buffer B as a blank. Concentrations were calculated using the theoretical absorption coefficient with all cysteine residues in disulfide linkages, as calculated by the protparam tool (<http://web.expasy.org/protparam>)¹⁴.

Anti-CD20 purification. 4 days post transient transfection of 293S and 293SGlycoDelete cells with the vector containing anti-CD20 (transient transfection, see online methods), the medium containing the expressed protein was harvested and loaded onto an affinity column 5ml HiTrap MabSelect SuRe (GE healthcare UK Ltd, Buckinghamshire, UK). The column was then washed with PBS until A₂₈₀ had dropped back to baseline. Bound proteins were eluted with 50 mM glycine pH 3,5 and collected in 1 ml fractions. The presence of anti-CD20 in the collected fractions was verified by tricine SDS-PAGE gel electrophoresis. We performed a buffer exchange on the pooled fractions that contained anti-CD20 to a 25 mM histidine 125 mM NaCl buffer at pH 6,0. Antibody concentration in the purified samples was measured with a Synergy MX spectrophotometer (Biotek, VT, USA). We measured the protein concentration based on the A₂₈₀ absorbance of the purified antibody. Concentrations were calculated using the theoretical extinction coefficient.

Supplementary Note 4: Methods in-gel tryptic digest

Gel pieces were 3 times washed with 50% acetonitrile (ACN), dried with 100% ACN and allowed to reswell in 100 mM NH₄HCO₃. After the third drying step, the 100 % ACN was discarded and the gel pieces were further dried in a speedvac. 750 ng of trypsin (Promega, Madison, WI, USA) was added and the gel pieces were allowed to reswell for 5 minutes. 100 mM NH₄HCO₃ was added to cover all gel pieces and the vials were incubated overnight at 37°C. 50 µl of 100 mM NH₄HCO₃ was added to each vial and the samples were incubated on a shaker for 15 minutes. Then, 50 µl of 100% ACN was added and vials were incubated on a shaker for 15 minutes. Supernatants were collected in fresh vials. 50 µl of 5% formic acid in 50% ACN/H₂O was added and the vials were incubated for 15 minutes on a shaker. The supernatants were collected. The 5% formic acid step was repeated once. Supernatants were pooled per sample and dried in a speedvac, then reconstituted with 20 µl of 50 mM phosphate buffer, pH 7.0 and 1 mM Pefabloc (Sigma-Aldrich).

Supplementary Note 5: Calculations ratio of sialylated or galactosylated glycans

To calculate the percentage of GlycoDelete glycans that are sialylated (trisaccharide), we extracted the area under the peak from the MALDI MS or LC-ESI-MS spectra for the Gal-GlcNAc-N and GlcNAc-N glycopeptides of both the undigested ($A_{GalGlcNAcUndig}$ and $A_{GlcNAcUndig}$) and α -2,3-sialidase digested ($A_{GalGlcNAcDig}$ and $A_{GlcNAcDig}$) GlycoDelete GM-CSF samples. The percentage of sialylated glycans was calculated as shown in the formula below. Gal-GlcNAc-N peak areas were first normalized to GlcNAc-N peak areas in both spectra. The resulting value for the Gal-GlcNAc-N peak from the undigested sample was subtracted from the value for the Gal-GlcNAc-N peak from the sialidase-digested sample. Then, this difference was divided by the summed normalized peak areas of the GlcNAc and GalGlcNAc peaks in the digested sample (the total normalized peak area of N27 or N37 encompassing glycopeptides).

$$\% \text{ sialylated glycans} = \frac{\left[\frac{A_{GalGlcNAcDig}}{A_{GlcNAcDig}} \right] - \left[\frac{A_{GalGlcNAcUndig}}{A_{GlcNAcUndig}} \right]}{\left[\frac{A_{GlcNAcDig}}{A_{GlcNAcDig}} \right] + \left[\frac{A_{GalGlcNAcDig}}{A_{GlcNAcDig}} \right]} * 100 \%$$

To calculate the percentage of GlycoDelete glycans that are galactosylated (disaccharide), the same datasets were utilized. The percentage of galactosylated glycans was calculated as shown in the formula below. Peak areas for Gal-GlcNAc-N were again first normalized in both the sialidase-digested and undigested samples. The normalized peak area for the undigested Gal-GlcNAc-N peak was then divided by the summed normalized peak areas of the GlcNAc-N and Gal-GlcNAc-N peaks in the digested sample (the total normalized peak area of N27 or N37 encompassing glycopeptides).

$$\% \text{ galactosylated glycans} = \frac{\left[\frac{A_{GalGlcNAcUndig}}{A_{GlcNAcUndig}} \right]}{\left[\frac{A_{GlcNAcDig}}{A_{GlcNAcDig}} \right] + \left[\frac{A_{GalGlcNAcDig}}{A_{GlcNAcDig}} \right]} * 100 \%$$

Supplementary Note 6: Biolayer interferometry assay.

Real-time binding of purified IgG to Fc γ RIIIaV was evaluated using biolayer interferometry (BLI) on an Octet RED96 system (Fortebio). Assays were performed at 30°C in kinetics buffer containing 1 mM of phosphate, 15 mM of NaCl, 0.002 (vol/vol) of Tween20, 0.005% (wt/vol) sodium azide, 0.1 mg/mL of BSA, pH 7.4. Fc γ RIIIaV (R&D Systems) tagged with a hexahistidine tag was brought to a concentration of 1.5 μ g/mL in kinetics buffer. The receptor was captured on an anti-Penta-His biosensor (Fortebio) for 10 minutes.

A first binding assay was performed with IgG at a single concentration of 50 μ g/mL in kinetics buffer. Association and dissociation were monitored for 5 minutes. Regeneration was performed by incubating the sensor with a 10 mM glycine pH 3.0 buffer for 20 s, followed by a 20 s incubation in kinetics buffer. These incubations were repeated twice.

For the kinetics experiment, an Fc γ RIIIaV-coated biosensor was incubated with IgG at concentrations ranging from 333 nM to 19 nM. A two minute baseline stabilization was followed by a 5 minutes association phase and a 15 minutes dissociation phase in kinetics buffer. Regeneration was performed as described above. The affinity was determined at equilibrium using the steady state model. Analyses was done using the ForteBio Data Analysis software (Fortebio).

References

1. Fenteany, F.H. & Colley, K.J. Multiple signals are required for alpha2,6-sialyltransferase (ST6Gal I) oligomerization and Golgi localization. *J. Biol. Chem.* **280**, 5423–5429 (2005).
2. Stanley, P. Chinese hamster ovary cell mutants with multiple glycosylation defects for production of glycoproteins with minimal carbohydrate heterogeneity. *Mol. Cell. Biol.* **9**, 377–383 (1989).
3. Stals, I. *et al.* Identification of a gene coding for a deglycosylating enzyme in *Hypocrea jecorina*. *FEMS Microbiol. Lett.* **303**, 9–17 (2010).
4. Grundmann, U., Nerlich, C., Rein, T. & Zettlmeissl, G. Complete cDNA sequence encoding human beta-galactoside alpha-2,6-sialyltransferase. *Nucleic Acids Res.* **18**, 667 (1990).
5. Nagata, Y. *et al.* Expression cloning of beta 1,4 N-acetylgalactosaminyltransferase cDNAs that determine the expression of GM2 and GD2 gangliosides. *J. Biol. Chem.* **267**, 12082–12089 (1992).
6. Laroy, W., Contreras, R. & Callewaert, N. Glycome mapping on DNA sequencing equipment. *Nat. Protoc.* **1**, 397–405 (2006).
7. Molday, R.S. & MacKenzie, D. Monoclonal antibodies to rhodopsin: characterization, cross-reactivity, and application as structural probes. *Biochemistry* **22**, 653–660 (1983).
8. Lockstone, H.E. Exon array data analysis using Affymetrix power tools and R statistical software. *Brief. Bioinformatics* **12**, 634–644 (2011).
9. Smyth, G.K. Linear Models and Empirical Bayes Methods for Assessing Differential Expression in Microarray Experiments. *Stat. Appl. Genet. Mol. Biol.* **3**, (2004).
10. Smyth, G.K., Michaud, J. & Scott, H.S. Use of within-array replicate spots for assessing differential expression in microarray experiments. *Bioinformatics* **21**, 2067–2075 (2005).
11. Smyth, G.K., Yang, Y.H. & Speed, T. Statistical issues in cDNA microarray data analysis. *Methods Mol. Biol.* **224**, 111–136 (2003).
12. Reiner, A., Yekutieli, D. & Benjamini, Y. Identifying differentially expressed genes using false discovery rate controlling procedures. *Bioinformatics* **19**, 368–375 (2003).
13. Schägger, H. Tricine-SDS-PAGE. *Nat. Protoc.* **1**, 16–22 (2006).
14. Gasteiger, E. *et al.* in *The Proteomics Protocols Handbook* (Walker, J. M.) 571–607 (Humana Press, 2005).